Adsorption
https://doi.org/10.1007/s10450-020-00255-y

Potentials and challenges of high-field PFG NMR diffusion studies with sorbates in nanoporous media

Amineh Baniani[1] · Samuel J. Berens[1] · Matthew P. Rivera[2] · Ryan P. Lively[2] · Sergey Vasenkov[1]

Received: 1 June 2020 / Revised: 30 July 2020 / Accepted: 12 August 2020
© Springer Science+Business Media, LLC, part of Springer Nature 2020

Abstract

High magnetic fields (up to 17.6 T) in combination with large magnetic field gradients (up to 25 T/m) were successfully utilized in pulsed field gradient (PFG) NMR studies of gas and liquid diffusion in nanoporous materials. In this mini-review, we present selected examples of such studies demonstrating the ability of high field PFG NMR to gain unique insights and differentiate between various types of diffusion. These examples include identifying and explaining an anomalous relationship between molecular size and self-diffusivity of gases in a zeolitic imidazolate framework (ZIF), as well as revealing and explaining an influence of mixing different linkers in a ZIF on gas self-diffusion. Different types of normal and restricted self-diffusion were quantified in hybrid membranes formed by dispersing ZIF crystals in polymers. High field PFG NMR studies of such membranes allowed observing and explaining an influence of the ZIF crystal confinement in a polymer on intra-ZIF self-diffusion of gases. This technique also allowed measuring and understanding anomalous single-file diffusion (SFD) of mixed sorbates. Furthermore, the presented examples demonstrate a high potential of combining high field PFG NMR with single-crystal infrared microscopy (IRM) for obtaining greater physical insights into the studied diffusion processes.

Keywords PFG NMR · High field NMR · Normal diffusion · Anomalous diffusion · ZIFs · MMMs

Notations

$\langle r^2 \rangle$	Mean square displacement
$\langle z^2 \rangle$	*Z*-Direction mean square displacement
c	Mass concentration
D	Self-diffusion coefficient
D_0	Corrected diffusion coefficient
D_T	Transport diffusion coefficient
D_{eff}	Effective diffusion coefficient
D_0^*	Pre-exponential factor in the Arrhenius equation for self-diffusion coefficient
d_{eff}	Diameter of spherical pores—see also Eq. 4
E_a	Activation energy of diffusion
F	Single-file mobility factor
g	Amplitude of the magnetic field gradient
l	Channel length
p	Pressure
p_i	PFG NMR signal fraction of component "*i*"—see Eq. 3
q	Constant defined as $\gamma g \delta$
R	Gas constant
S	PFG NMR signal intensity
t	Diffusion time
T	Temperature
T_1	Longitudinal NMR relaxation time
T_2	Transverse NMR relaxation time
γ	Gyromagnetic ratio
Γ	Thermodynamic factor equal to $d\ln(p)/d\ln(c)$
δ	Effective gradient pulse duration corresponding to the width of the gradient pulses with a rectangular shape
θ	Fractional loading in the channels
λ	Particle elementary displacement
Ψ	Attenuation of PFG NMR signal

1 Introduction

The majority of reported NMR diffusion studies in nanoporous materials have been performed using low to midfield NMR instruments (Kärger et al. 2012). This was mostly

✉ Sergey Vasenkov
svasenkov@che.ufl.edu

[1] Department of Chemical Engineering, University of Florida, Gainesville, FL 32611, USA

[2] School of Chemical & Biomolecular Engineering, Georgia Institute of Technology, Atlanta, GA 30332, USA

Published online: 25 August 2020

done to decrease limitations resulting from disturbing magnetic susceptibility effects, which become less severe with decreasing magnetic field strength (Callaghan et al. 1991). For molecules diffusing in nanoporous solids such effects can further decrease proton T_2 NMR relaxation times, which are already shortened by confinement effects in nanopores. Short T_2 NMR relaxation times is one of the most common reasons for a failure to perform NMR diffusion studies in nanoporous samples (Kärger et al. 2012). This limitation can be overcome by using other types of nuclei, which exhibit much longer T_2 NMR relaxation times even under conditions of restricted mobility in confining pores. The well-known examples of such nuclei are ^{13}C and ^{129}Xe. It is important to note, however, that the signal-to-noise ratios in diffusion NMR studies performed with ^{13}C and ^{129}Xe at low- and mid-field can become too low for obtaining meaningful diffusion data. We use high (up to 17.6 T) magnetic field in ^{13}C and ^{129}Xe pulsed field gradient (PFG) NMR diffusion studies to increase signal-to-noise ratios, which become larger with increasing field strength (Forman et al. 2017, 2019, 2020; Mueller et al. 2016, 2015; Baniani et al. 2019; Berens et al. 2018, 2019; Dutta et al. 2015, 2016). As a result, using high field allows performing high-sensitivity diffusion studies with the ^{13}C and ^{129}Xe detection when there are no disturbing effects, such as chemical shift anisotropy relaxation effects, leading to a significantly faster NMR relaxation at a larger field. Hence, the ^{13}C and ^{129}Xe detection leads to a possibility of performing diffusion measurements even under the conditions of severe confinement effects in nanopores resulting in the proton T_2 NMR relaxation times that are too-short for PFG NMR measurements. The problem with short T_2 NMR relaxation times in NMR diffusion studies of porous materials can also be addressed by using magic angle spinning (MAS) PFG NMR (Freude et al. 2019; Dutta et al. 2018a) and q-space singlet NMR (Torres et al. 2020). However, the former technique is limited by relatively small (around 1 T/m) maximum gradient strength, while the latter can only be used for molecules exhibiting long-lived singlet spin order.

Owing to the application of high field, it often becomes possible to verify our diffusion data by comparing the results obtained for the same samples and sorbates with different types of nuclei (^{13}C and ^{1}H) (Forman et al. 2019, 2020, 2017; Baniani et al. 2019; Berens et al. 2018). The diffusion results can also be routinely verified by comparing data measured with the same type of nuclei at high and low/midrange magnetic field strengths (Forman et al. 2017, 2020, 2019; Baniani et al. 2019; Berens et al. 2018, 2019). An observation of an agreement of the diffusion data measured with different nuclei and/or field strengths results in a high degree of reliability of our data. In the remainder of this mini-review we summarize some recent examples of our high field PFG NMR studies highlighting applicability of this technique for diffusion studies in nanoporous solids. Basics of PFG NMR and its application for diffusion studies in porous materials are presented in this special issue by Kärger et al. (2020) as well as in previously published books (Kärger et al. 2012; Price 2009; Callaghan 2011; Stilbs 2019). It is important to note that PFG NMR, pulsed gradient spin echo (PGSE) NMR, and NMR diffusometry are used synonymously by many researches.

2 Selected relations used in PFG NMR

In this section, we summarize relations used in the discussed below PFG NMR studies. Please see Kärger et al. (2020) in this issue for a comprehensive review of the PFG NMR technique. In PFG NMR, self-diffusivities and related mean square displacements (MSDs) are commonly obtained from attenuation curves, viz. the dependences of the normalized PFG NMR signal intensity (S) on the amplitude of the magnetic field gradient (g). PFG NMR attenuation curves for normal 3-dimensional self-diffusion with a single self-diffusion coefficient (D) can be presented as (Kärger et al. 2012, 1988, 2020; Callaghan et al. 1991)

$$\Psi = \frac{S(g)}{S(g \approx 0)} = \exp\left(-\frac{\langle r^2(t)\rangle q^2}{6}\right) = \exp(-Dq^2 t), \qquad (1)$$

where Ψ is the attenuation of PFG NMR signal, $\langle r^2(t)\rangle$ denotes MSD, t is the diffusion time, and $q = \gamma g \delta$, where γ is the gyromagnetic ratio, and δ is the effective gradient pulse duration corresponding to the width of the gradient pulses with a rectangular shape (Kärger et al. 2012, 2020). The right-hand part of Eq. 1 is written using the Einstein relation

$$\langle r^2(t)\rangle = 2nDt, \qquad (2)$$

where $n = 1$, 2, and 3, respectively, for one-dimensional, two-dimensional and three-dimensional diffusion process.

PFG NMR attenuation curves for two ensembles of molecules diffusing with different diffusivities can be presented as (Kärger et al. 1988, 2012, 2020)

$$\Psi = \frac{S(g)}{S(g \approx 0)} = \sum_{i=1}^{2} p_i \exp(-D_i q^2 t), \qquad (3)$$

where p_i and D_i are the phase fraction (i.e. PFG NMR signal fraction) and self-diffusion coefficient of ensemble i ($i = 1$ or 2), respectively.

For the case of restricted diffusion in spherical pores of diameter d_{eff}, Eq. 1 can be re-written as (Stallmach and Kärger 1999; Kärger et al. 2020)

$$\Psi = \frac{S(g)}{S(g \approx 0)} = \exp\left(-\frac{d_{eff}^2(t)q^2}{20}\right). \quad (4)$$

In the case of single-file diffusion, one dimensional diffusion in non-intersecting channels that are so narrow that mutual passages of diffusing molecules are excluded, the MSD dependence on diffusion time deviates from Eq. 2. For channels, which are so long that any boundary effects at the channel ends can be neglected, MSD is expected to obey the following relation (Kärger et al. 2012)

$$\langle z^2(t)\rangle = 2Ft^{0.5}, \quad (5)$$

where F is the single-file mobility factor.

Using Eq. 5, the PFG NMR signal attenuation for straight, randomly oriented single-file channels can be presented as (Kärger et al. 2012; Dvoyashkin et al. 2013)

$$\Psi(q,t) = \sqrt{\frac{\pi}{2q^2\langle z^2(t)\rangle}}erf\left(\sqrt{\frac{q^2\langle z^2(t)\rangle}{2}}\right) = \sqrt{\frac{\pi}{4q^2Ft^{0.5}}}erf\left(\sqrt{q^2Ft^{0.5}}\right), \quad (6)$$

where $q = \gamma g \delta$.

3 Manifestation of structural flexibility of zeolitic imidazolate frameworks (ZIFs) in intra-ZIF gas diffusion

Zeolitic imidazolate frameworks (ZIFs), a type of metal organic frameworks (MOFs) with zeolite-like topologies, have emerged as attractive materials for gas separation. ZIFs are generally composed of tetrahedral metal centers that are typically fully coordinated to organic ligands resulting in microporous structures. Due to high stability, large surface area, and tunable pore aperture, ZIFs have potential to serve as molecular sieves (Park et al. 2006; Banerjee et al. 2008; Zhang et al. 2012b; Phan et al. 2010; Thompson et al. 2012). In contrast to zeolites, significant framework flexibility of ZIFs allows for an intracrystalline diffusion of guest molecules that have sizes larger than the nominal ZIF pore aperture size. Since framework flexibility can drastically affect intra-ZIF diffusion of guest molecules, detailed knowledge of the role of this flexibility in molecular diffusion is required for potential applications of ZIFs in separations as well in any other applications involving molecular diffusion including catalysis and sensor development.

Composed of benzimidazolate linkers and Zn^{2+} metal centers, ZIF-11 (3.0 Å Banerjee et al. 2008; Park et al. 2006) has been studied for its potential in separation of small molecules (Kortunov et al. 2011; Sánchez-Laínez et al. 2015; Park et al. 2006; Forman et al. 2017; Pimentel et al. 2019). Owing to this interest, we have carried out a self-diffusion study of mixed and pure C_2H_6 (~4.4 Å Li et al. 2009) and C_2H_4 (~4.2 Å Li et al. 2009) in ZIF-11 by ^{13}C and ^{1}H PFG NMR at 14 and 17.6 T (Baniani et al. 2019). The PFG NMR measurements were performed with different batches of ZIF-11 crystals for a broad range of root MSDs at different temperatures and gas concentrations. In the PFG NMR measurements, a combination of high field (14 or 17.6 T) and large magnetic field gradient strength (up to 25 T/m) allowed measuring self-diffusivities corresponding to length scales smaller than the average ZIF-11 crystal size for all studied crystal batches. Complementary diffusion measurements were carried out by IR microscopy (IRM) and standard volumetric uptake technique on large (~100 µm) ZIF-11 crystal batch. Due to technique limitations, only large crystal batch was used in IRM and volumetric uptake measurements (Baniani et al. 2019).

Figure 1 shows an overview of the intracrystalline self-diffusivities of C_2H_6 and C_2H_4 measured in ZIF-11 by PFG NMR at 296 K as a function of the total gas concentration in the crystals (Baniani et al. 2019). It can be seen in Fig. 1 that for single sorbate samples, larger C_2H_6 molecules (square symbols) diffuse faster than smaller C_2H_4 molecules (triangle symbols) at all concentrations greater than 0.5 mmol/g. This anomalous relationship between the molecular size and self-diffusivity was observed in the data measured for

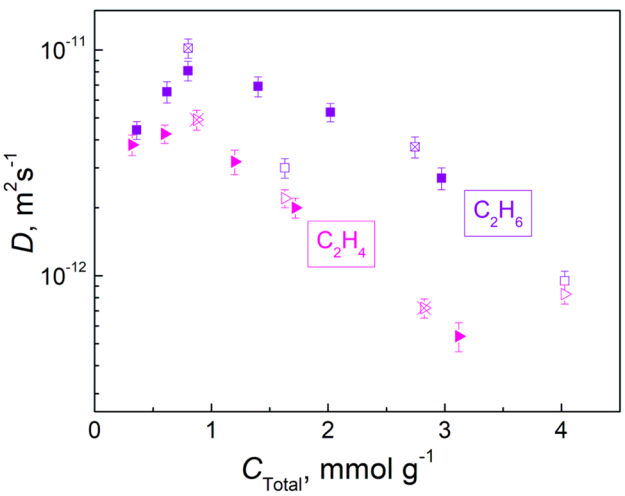

Fig. 1 Concentration dependence of intracrystalline self-diffusivities of C_2H_6 (square symbols) and C_2H_4 (triangle symbols) in ZIF-11 crystal beds measured by PFG NMR at 296 K for the smallest diffusion times. Filled and hollow symbols with crosses corresponds to the data obtained for the single sorbates in the small (~3–5 µm) and large (~100 µm) ZIF-11 crystal batches, respectively. Hollow symbols correspond to the approximately equimolar C_2H_6/C_2H_4 mixtures in the small ZIF-11 crystal batch. For the mixture samples, the concentration shown in the figure corresponds to the combined concentration of both gases

different diffusion times. The observed self-diffusivity independence of the diffusion time at sufficiently small time values confirmed an absence of any disturbing effects at the external surface of ZIF-11 crystals for these diffusion times (Baniani et al. 2019). The absence of such surface effects under our experimental conditions at small times was also confirmed by the satisfactory agreement of the gas intracrystalline self-diffusivities in the small (~ 3–5 μm, filled symbols in Fig. 1) and large (~ 100 μm, hollow symbols with crosses in Fig. 1) ZIF-11 crystals at the same or similar gas loadings and the same temperature. This consistency in the diffusion data clearly demonstrates that any disturbing effects related to the size of the crystals do not contribute to the observed anomalous relationship between the molecular size and self-diffusivity. For mixed C_2H_6/C_2H_4 gas samples, it was observed that replacing a fraction of C_2H_6 with C_2H_4 results in a decrease of the intracrystalline self-diffusivity of the remaining C_2H_6 molecules (hollow symbols in Fig. 1). All of these data were explained by an interaction of C_2H_4 with ZIF-11 linkers which reduces ZIF-11 framework flexibility and, as a result, makes the effective or maximum aperture size of ZIF-11 crystals smaller (Baniani et al. 2019).

Furthermore, clear trends in the concentration dependence of the self-diffusivities of C_2H_6 and C_2H_4 in ZIF-11 can be seen in Fig. 1. At small concentrations, the self-diffusivities of C_2H_6 and C_2H_4 increase with increasing sorbate concentration. This can be explained by the expectation that the lowest free energy sites in ZIF-11 are filling up first (Baniani et al. 2019; Kortunov et al. 2011). Indeed, the residence times of gas molecules in such sites are expected to be longer than those in the remaining ZIF-11 sites corresponding to weaker gas–framework interactions. At large concentrations, the self-diffusivities of C_2H_6 and C_2H_4 decrease with increasing sorbate concentration. This can happen due to mutual hindrance of the molecules in confining micropores of ZIF-11. Similar concentration dependencies and their explanation were reported for zeolites (Kärger et al. 2012, 2020). In the case of ZIF-11, it is also possible to explain such concentration dependence by a reduction in a framework flexibility due to molecular crowding, which leaves little or no free volume for linkers to re-orient when the gas concentration is sufficiently large (Baniani et al. 2019; Kortunov et al. 2011). Such reduction in the linker and aperture flexibility can lead to a decrease in the intra-ZIF self-diffusivity of gas molecules, in agreement with the observed trend at high gas concentrations (Fig. 1).

Self-diffusion of C_2H_6 and C_2H_4 in ZIF-11 was also studied as a function of temperature using ^1H and ^{13}C high field PFG NMR (Fig. 2) (Baniani et al. 2019). Coincidence of the diffusion data measured with different nuclei types (^1H and ^{13}C) under the same conditions and for the same samples rules out any measurement artifacts in the data shown in Fig. 2. In order to obtain diffusion data for the same

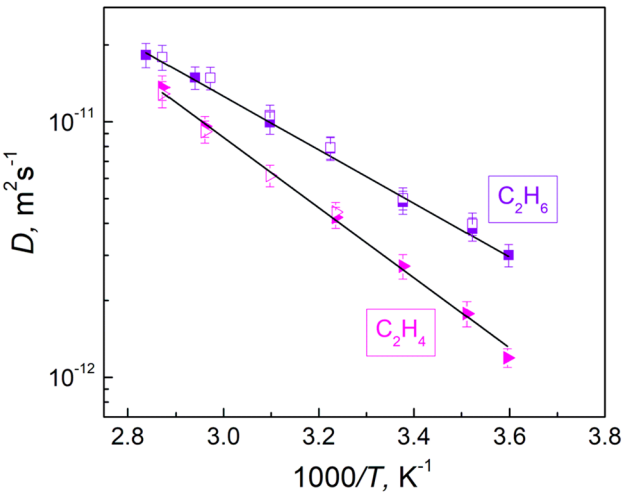

Fig. 2 Intracrystalline self-diffusivities of C_2H_6 (square symbols) and C_2H_4 (triangle symbols) in ZIF-11 crystal beds as a function of temperature measured by PFG NMR. The diffusion measurements were performed using ^1H (filled symbols) and ^{13}C (hollow symbols) resonances under the conditions of the same or similar intra-ZIF concentrations and MSDs for each sorbate. The data were measured with the small (~ 3–5 μm) crystal batch

intra-ZIF concentrations at different temperatures, several samples with different sorbate loadings were prepared and studied. It was observed that the temperature dependence of the self-diffusivities of C_2H_6 and C_2H_4 can be described by Arrhenius law, $D(T) = D_0^* \exp\left(-\frac{E_a}{RT}\right)$, where $D_0{}^*$ is the pre-exponential factor and E_a is the activation energy of diffusion. It can be seen in Fig. 2 that the temperature dependence slopes indicate larger activation energy of diffusion for C_2H_4 than for C_2H_6. These activation energies were found to be equal to 26.3 kJ/mol and 20.0 kJ/mol for C_2H_4 and for C_2H_6, respectively (Baniani et al. 2019). Larger activation energy for C_2H_4 than for C_2H_6 is consistent with the discussed above reduction in the framework flexibility and the related reduction in the maximum or effective aperture size in ZIF-11 due to the presence of C_2H_4 (Baniani et al. 2019). Indeed, the activation energy of diffusion is expected to be larger when the aperture size is smaller.

To confirm the anomalous relationship between the C_2H_6 and C_2H_4 self-diffusivities and their molecular sizes observed by high field PFG NMR, complementary diffusion measurements were performed by IRM and macroscopic volumetric uptake technique (Baniani et al. 2019). These measurements were performed under the same or similar experimental conditions as those used in the discussed above PFG NMR studies. It is important to note that both IRM and volumetric uptake technique yield transport diffusivities (D_T). While the former technique allowed obtaining transport diffusivity in selected single ZIF-11 crystals, the latter provided average transport

diffusivity for a bed of ZIF-11 crystals (Baniani et al. 2019). In order to compare the transport diffusion data obtained by IRM and volumetric technique with the self-diffusivities measured by high field PFG NMR, Darken equation $D_T = D_0 \frac{d\ln(p)}{d\ln(c)} = D_0\Gamma$ (Kärger et al. 2012, 2003) was used. This equation allowed obtaining corrected diffusivities (D_0), which can be directly compared with self-diffusivities, because self-diffusivities and corrected diffusivities are expected to coincide for the studied porous system (Baniani et al. 2019). For each measured transport diffusivity, the corresponding value of D_0 was calculated using the thermodynamic factor (Γ) resulting from the adsorption isotherms $c(p)$ for ZIF-11. Figure 3 shows an overview of all the diffusion data obtained by high field PFG NMR, IRM and volumetric technique. In this figure, filled and hollow symbols with crosses correspond to the PFG NMR data, hollow symbols correspond to the IRM data and half-filled symbols show the volumetric technique data. It can be seen in Fig. 3 that the corresponding data obtained by different techniques are consistent with each other, within uncertainty. This observation further confirms the previously discussed PFG NMR results and their interpretation (Baniani et al. 2019).

An emerging strategy for improving ZIF's separation performance is based on tuning the pore aperture size by mixing two differently-sized organic linkers in the same framework (Eum et al. 2015; Hillman et al. 2018, 2017; Thompson et al. 2012). One such example is ZIF-7–8, a mixed-linker ZIF with 2-methylimidazole (ZIF-8) and benzimidazole (ZIF-7) linker types tetrahedrally coordinated in the framework with Zn^{2+} ions (Hillman et al. 2018, 2017; Berens et al. 2018, 2019). In comparison to ZIF-8, a slightly smaller pore aperture size is expected in ZIF-7–8. As the effective pore aperture size of ZIF-7–8 is estimated to be roughly similar to the size of C_2H_4 and C_2H_6 and slightly larger than CO_2 and CH_4, high field PFG NMR can be used to detect differences in self-diffusion of these gases in order to evaluate the potential for gas separations with ZIF-7–8.

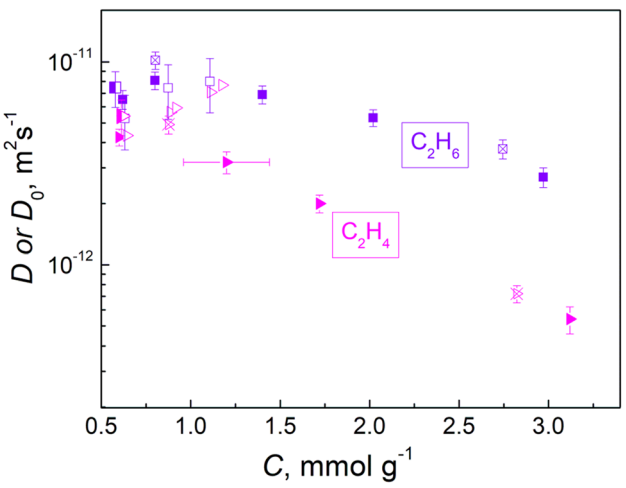

Fig. 3 Comparison of the self-diffusivities and corrected diffusivities measured in ZIF-11 crystals for different intracrystalline concentrations of C_2H_6 (square symbols) or C_2H_4 (triangle symbols). Filled symbols and hollow symbols with crosses corresponds to the self-diffusivities measured by PFG NMR at 296 K in the small (~3–5 μm) and large (~100 μm) ZIF-11 crystal batches, respectively. Hollow symbols correspond to the corrected diffusivities measured by IRM at 298 K in the large ZIF-11 crystal batch. Half-filled symbols correspond to the corrected diffusivities measured by the volumetric technique at 296 K in the large ZIF-11 crystal batch

Multinuclear (^{1}H, ^{13}C, and ^{129}Xe) high field PFG NMR at both 14 and 17.6 T was utilized in order to perform pure and mixed gas self-diffusion measurements on ZIF-7–8 (Berens et al. 2018, 2019). To our knowledge, these measurements represent first time microscopic studies of pure and mixed gas self-diffusion in a mixed-linker MOF of any type. Primarily, ^{13}C PFG NMR was used as it benefits from the ^{13}C T_2 NMR times, which are sufficiently long (between 5 and 29 ms) for all studied gases. As ^{13}C was necessary to achieve relatively long T_2 relaxation times resulting in a smaller reduction of the PFG NMR signal of gas molecules due to T_2 NMR relaxation process, the application of the high magnetic field helped compensate for the small sensitivity of ^{13}C NMR in comparison to the more traditional ^{1}H NMR.

Figure 4 shows attenuation curves of the four studied gases in both ZIF-8 and ZIF-7–8 at 296 K. In contrast to the monoexponential (linear in the presentation of the figure) attenuation in agreement with Eq. 1 in the ZIF-8 samples, all the attenuation curves measured for ZIF-7–8 exhibit deviations from the monoexponential behavior. An absence of any measurement artifacts was confirmed by comparing the diffusion data measured on the 14 T spectrometer with a *Diff30* diffusion probe with those measured on the 17.6 T spectrometer with a *Diff50* diffusion probe. The crossed symbols in Fig. 4a show data measured at 17.6 T that coincide with the hollow symbols corresponding to the data collected at 14 T for the same samples and conditions. This coincidence indicates the absence of possible trivial hardware issues or inherent magnetic susceptibility artifacts. Furthermore, ^{1}H PFG NMR data (filled symbols in the initial attenuation range of Fig. 4a) also show consistency with the corresponding ^{13}C PFG NMR data for the same sample and conditions indicating no dependence on the nuclei type used for the diffusion measurements.

The attenuation curves for ZIF-7–8 crystals coincide, within uncertainty, across a broad range of diffusion times (Fig. 4) indicating essentially identical self-diffusivities for different length scales of displacements inside any particular crystal. At the same time, deviations of the attenuation curves measured for ZIF-7–8 samples from the monoexponential behavior point out at an existence of a distribution over the gas self-diffusivities in these samples. As a result, it

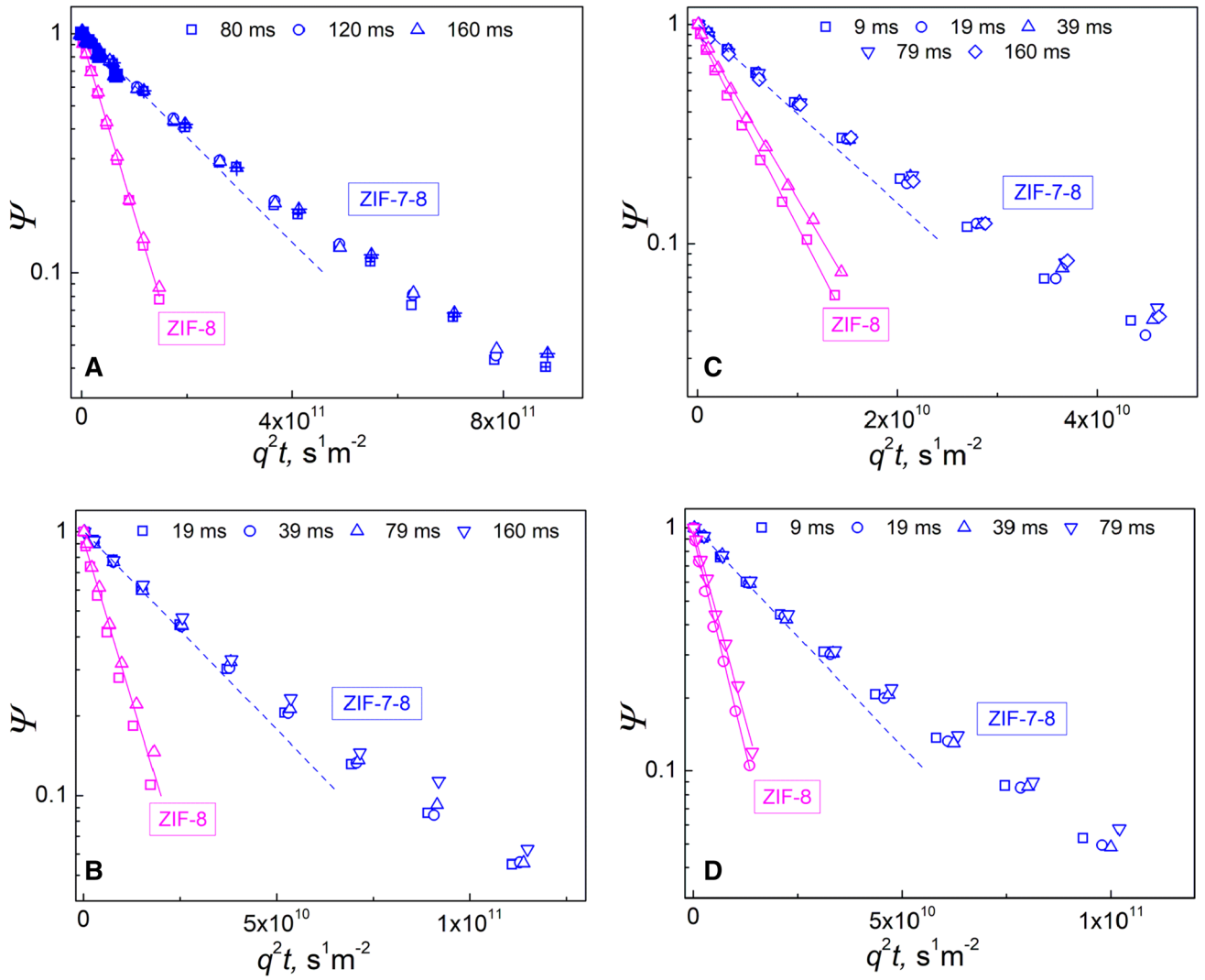

Fig. 4 Representative ^{13}C PFG NMR attenuation curves for self-diffusion of C_2H_6 (**a**), C_2H_4 (**b**), CO_2 (**c**), and CH_4 (**d**) in ZIF-7–8 and ZIF-8 at 296 K. C_2H_6 was loaded at 2.7 bar, and the other gases were loaded at around 7.8 bar at 296 K. ^1H PFG NMR attenuation curves (filled symbols) are also shown for C_2H_6 diffusion in ZIF-7–8 for a range of small attenuation values. Solid lines represent a monoexponential fit of the ZIF-8 attenuation curves using Eq. 1. Dashed lines represent a monoexponential fit of the initial parts ($\Psi \geq 0.3$) of the ZIF-7–8 attenuation curves using Eq. 1. Crossed C_2H_6 data points were measured at 17.6 T. All other data was measured at 14 T

was concluded that the deviations from the monoexponential behavior arose from differences in self-diffusivity between different ZIF-7–8 crystals (Berens et al. 2018, 2019). This distribution of diffusivities was confirmed by complementary single crystal IRM measurements in which the transport diffusivity of C_2H_6 was found to vary significantly between different individual crystals of ZIF-7–8 (Berens et al. 2018). Additionally, when the Darken equation was used, as discussed above, to calculate corrected diffusivities (D_0) from the transport diffusivities measured by IRM, a good agreement was observed between the corresponding D_0 values and the effective self-diffusivity (D_{eff}) values from PFG NMR (Fig. 5). The latter self-diffusivities were obtained from the initial slopes of the PFG NMR curves using Eq. 1. These diffusivities represent average or characteristic diffusivities in macroscopic PFG NMR samples containing many ZIF-7–8 crystals. The agreement observed between the corresponding values of D_0 and D_{eff} (Fig. 5) further confirms an absence of any measurements artifacts or disturbing effects at the external crystal surface which can lead to distortions in apparent D_0 and D_{eff} values for intracrystalline diffusion. The distribution widths over the values of the corrected and self-diffusivities estimated from the IRM and PFG NMR data for the studied batch of ZIF-7–8 crystals were also found to be in a good agreement (Berens et al. 2018). Furthermore, it is important to note the powerful complement between single crystal IRM and high field PFG NMR, as the former can probe transport diffusion in any single selected

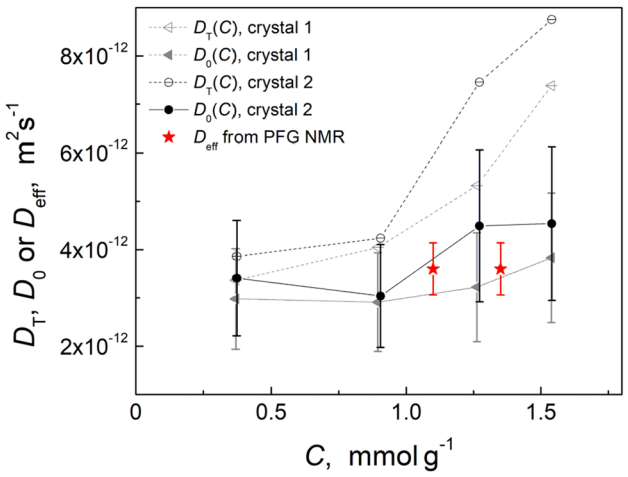

Fig. 5 Comparison of the transport (D_T), corrected (D_0), and self- (D_{eff}) diffusivities of C_2H_6 inside ZIF-7–8 crystals. IRM at 298 ± 1 K was utilized to obtain D_T, and the corresponding D_0 values for selected single crystals of ZIF-7–8. D_{eff} was measured with PFG NMR at 296 ± 1 K

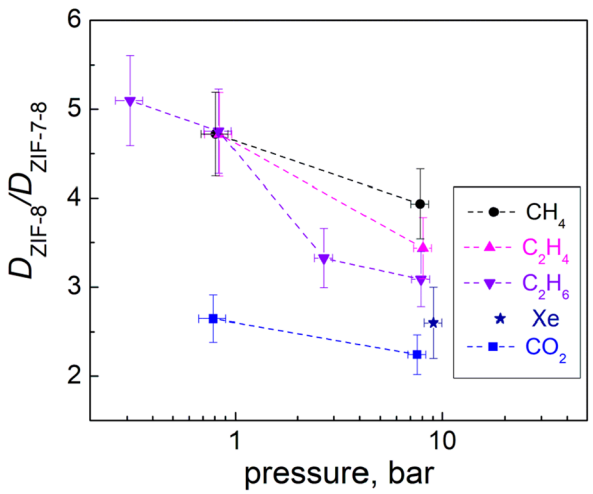

Fig. 6 Ratios of the gas self-diffusivity in ZIF-8 and effective self-diffusivity in ZIF-7–8 for different gases as a function of the gas loading pressure at 296 K

crystal and the latter can allow for measurements of intracrystalline self-diffusion behavior for a broad range of length scales smaller than the crystals size in a macroscopic sample containing many such crystals.

To evaluate differences in diffusion properties of ZIF-8 and ZIF-7–8, the values of the effective self-diffusivities measured for gas diffusion in ZIF-7–8 ($D_{ZIF-7-8}$) were compared with the corresponding self-diffusivities in ZIF-8 (D_{ZIF-8}) by plotting the ratios $D_{ZIF-8}/D_{ZIF-7-8}$ for different gas loading pressures at 296 K (Fig. 6). The data in Fig. 6 makes it apparent that $D_{ZIF-7-8}$is significantly lower for all gases than the corresponding value of D_{ZIF-8}, which is consistent with permeation measurements (Hillman et al. 2018) and the expectation that smaller pore apertures of ZIF-7–8 slows down the diffusion process in comparison to that in ZIF-8. As discussed above, ZIF frameworks often exhibit flexibility, which can influence intra-ZIF self-diffusivities of gas molecules (Haldoupis et al. 2012; Parkes et al. 2014; Baniani et al. 2019; Diestel et al. 2015; Forman et al. 2019, 2020). The data in Fig. 6 provide evidence that framework flexibility can impact gas self-diffusion more in ZIF-7–8 than in ZIF-8 at high gas loading pressures of around 8 bar. Indeed, if the frameworks of both ZIFs were completely rigid, increasing values of $D_{ZIF-8}/D_{ZIF-7-8}$would be generally expected with increasing sorbate size and otherwise the same or similar conditions owing to the larger in ZIF-8 than in ZIF-7–8 aperture size. However, for sorbates larger than CO_2 at around 8 bar, there is no increase in the diffusivity ratio with increasing sorbate size (Fig. 6). In fact, that data in Fig. 6 indicate that at large loading pressures the values of $D_{ZIF-8}/D_{ZIF-7-8}$show a tendency to decrease with an increasing sorbate size for molecules larger than CO_2. In particular, it can be seen that this ratio is larger for CH_4 (~3.8 Å Pantatosaki et al. 2011) than for Xe (~4.1 Å Li et al. 2009; Banerjee et al. 2017). These data indicate a significant extent of framework flexibility in ZIF-7–8, where larger molecules appear to have an ability to distort/expand the apertures to a larger extent resulting in faster diffusion of these molecules.

These framework flexibility effects on self-diffusion were also apparent in the diffusion selectivity, which can be defined as a ratio of the self-diffusivities of two gases in the same porous material ($S_{gas1/gas2} = D_{gas1}/D_{gas2}$) (Berens et al. 2019). Given a completely rigid framework, the smaller pore aperture size of ZIF-7–8 should lead to an increase in the value of S in ZIF-7–8 relative to ZIF-8. For the smaller sorbates CO_2 and CH_4, S_{CO_2/CH_4} was indeed found to be around a factor of 2 larger for ZIF-7–8 than for ZIF-8. However, in the case of the larger C_2H_4 and C_2H_6, $S_{C_2H_4/C_2H_6}$ was found to be the same, within uncertainty, for both ZIFs (Berens et al. 2019). These data confirm that ZIF-7–8 experiences significant framework flexibility effects, such as distortions in the size and/or shape of pore apertures in the presence of large sorbate molecules at sufficiently large sorbate concentrations. These effects manifest themselves in greater than expected self-diffusivities of large gas molecules in ZIF-7–8.

4 Sorbate diffusion in MOF–polymer hybrid membranes

Membrane-based separation technology is an attractive alternative to the traditional distillation technology due to the expectation of lower operating costs and energy consumption associated with membrane-based separations (Baker 2002; Pandey and Chauhan 2001; Bernardo et al.

2009). One promising type of gas-separation membranes is mixed-matrix membranes (MMMs). MMMs are formed by incorporating filler (i.e. molecular sieve) particles in a pure polymeric film. MMMs benefit from combining superior separation properties of filler particles with good mechanical properties of pure polymeric films (Zhang et al. 2012a, 2008; Zornoza et al. 2011; Yilmaz and Keskin 2012; Ordoñez et al. 2010). MOFs and ZIFs are promising candidates for a filler.

Previous experimental and simulation studies of ZIF-based MMMs showed improved performance of MMMs for gas separations compared to their base polymeric matrices (Ordoñez et al. 2010; Yilmaz and Keskin 2012; Zhang et al. 2012a; Bae et al. 2010; Díaz et al. 2011; Li et al. 2013; Diestel et al. 2015). A common approach to characterize transport properties of such MMMs is based on macroscopic permeation measurements where gas fluxes through an entire membrane are measured as a function of the pressure gradient across the membrane. This approach, however, cannot directly resolve diffusion in the ZIF and polymer phases of MMMs. We have recently demonstrated that such resolution can be achieved using high field PFG NMR for both pure and mixed gases (Mueller et al. 2015, 2016; Forman et al. 2019, 2020). An ability to measure gas self-diffusion inside ZIF crystals embedded in polymers by high field PFG NMR led to an important observation concerning intra-ZIF diffusion. It was found that confinement of ZIF crystals in certain types of polymers can change intra-ZIF self-diffusivity of gas molecules. These results are discussed in more detail below.

Initially, a small effect of confinement of ZIF-8 crystals in 6FDA-DAM polymer on intra-ZIF self-diffusion of C_2H_6 and C_2H_4 was observed by PFG NMR (Mueller et al. 2015, 2016). In this study, the observed small (~ 30%) reduction in the intra-ZIF gas self-diffusivity in the MMM in comparison to the corresponding self-diffusivity in a ZIF-8 bed was explained by a reduction in ZIF-8 framework flexibility induced by the confinement in the polymer. To further investigate this confinement effect, we extended our high field PFG NMR measurements to MMMs formed with ZIF-11, the material that demonstrates large framework flexibility effects, as discussed above. Self-diffusion of C_2H_6 and C_2H_4 was studied inside three ZIF-11 based MMMs with base polymers Torlon, Matrimid and 6FDA-DAM at different temperatures and gas concentrations (Forman et al. 2019, 2020). All studied MMMs demonstrate a good adhesion between polymer and ZIF-11 crystals as observed by SEM. An example of a SEM image for one of the studied MMMs (ZIF-11/Matrimid MMM) is shown in Fig. 7a. Measured intra-ZIF self-diffusivities in the MMMs were compared with the corresponding self-diffusivities in beds of ZIF-11 crystal from the same batches as those used to produce these MMMs. These measurements were performed using multinuclear (^{13}C and ^{1}H) PFG NMR at high field (14 or 17.6 T) and using large magnetic field gradients (up to 25 T/m) to record self-diffusivities inside ZIF-11 crystals for displacements smaller than the mean crystal size. Figure 7b shows examples of the measured PFG NMR attenuation curves for self-diffusion of C_2H_6 in ZIF-11/Torlon MMM and its respective ZIF-11 crystal bed. For this MMM as well as for ZIF-11/Matrimid MMM, only intra-ZIF diffusion contributed to the measured attenuation curves. This happened because the T_2 NMR relaxation times of the studied gases in the polymer phases of these MMMs were found to be too small for an observation of any intra-polymer PFG NMR signal under our experimental conditions. As a result, the measured attenuation curves for these two MMMs were monoexponential in agreement with Eq. 1, i.e. linear in the presentation of Fig. 7b, indicating a single gas self-diffusion coefficient measured for each MMM under any particular experimental conditions. For the remaining MMM, ZIF-11/6FDA-DAM MMM, the T_2 NMR relaxation times of the studied gases in the polymer phase were appreciably larger (Forman et al. 2019, 2020), leading to a contribution of the intra-polymer diffusion into the measured PFG NMR attenuation curves. Figure 7c shows examples of the measured PFG NMR attenuation curves for the self-diffusion of C_2H_6 in ZIF-11/6FDA-DAM MMM, its respective ZIF-11 crystal bed, and pure 6FDA-DAM polymer film. The deviations of the shape of the attenuation curves in ZIF-11/6FDA-DAM MMM from the monoexponential one, i.e. linear in the presentation of Fig. 7c, were found to be in a quantitative agreement with Eq. 3, which describes the case of separate contributions from the intra-ZIF and intra-polymer diffusion of gas molecules into the measured attenuation curves (Forman et al. 2020). Using Eq. 3, both intra-ZIF and intra-polymer gas self-diffusivities were obtained for this MMM. The ratios of the intra-ZIF self-diffusivities in ZIF-11 crystal beds (D_{bed}) to those in the ZIF-11 based MMMs (D_{MMM}) were examined quantitatively and presented in Fig. 8 for C_2H_6 (filled symbols) and C_2H_4 (hollow symbols) as a function of the gas loading pressure at 296 K (Forman et al. 2020, 2019). It can be seen in Fig. 8 that at the lowest and intermediate sorbate loading pressures, intra-ZIF self-diffusivity in beds of ZIF-11 crystals is larger than the corresponding intra-ZIF self-diffusivity in ZIF-11/Torlon MMM for both C_2H_6 and C_2H_4. Larger intra-ZIF self-diffusivity observed for ZIF-11 crystal bed in comparison to intra-ZIF self-diffusivity in ZIF-11/Torlon MMM was explained by the ZIF-11 framework flexibility reduction resulting from the confinement of ZIF-11 crystals in Torlon polymer. At the same time, for the other two studied MMMs, the intra-ZIF self-diffusivity in the MMMs was found to be the same, within uncertainty,

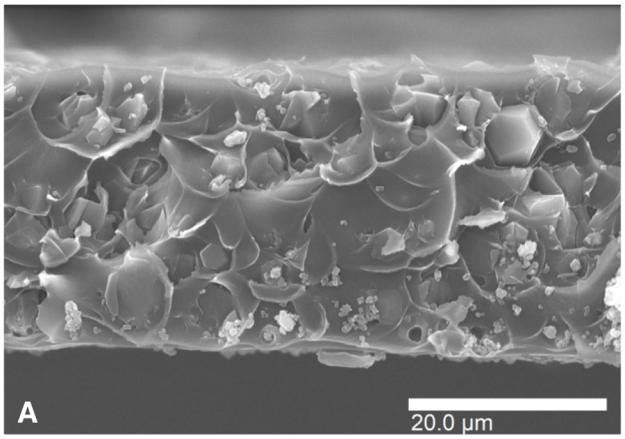

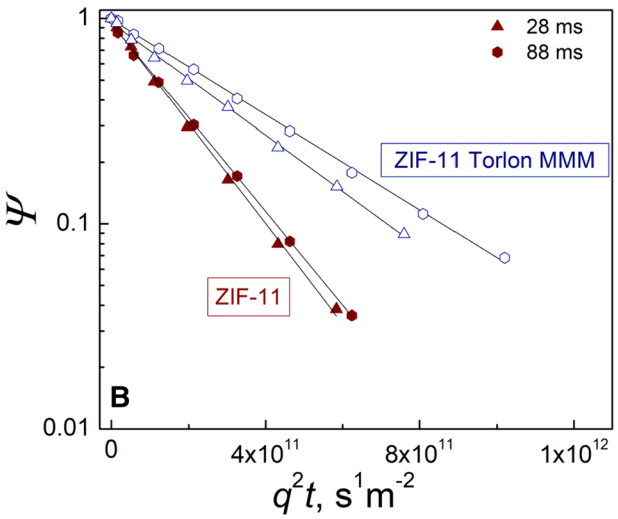

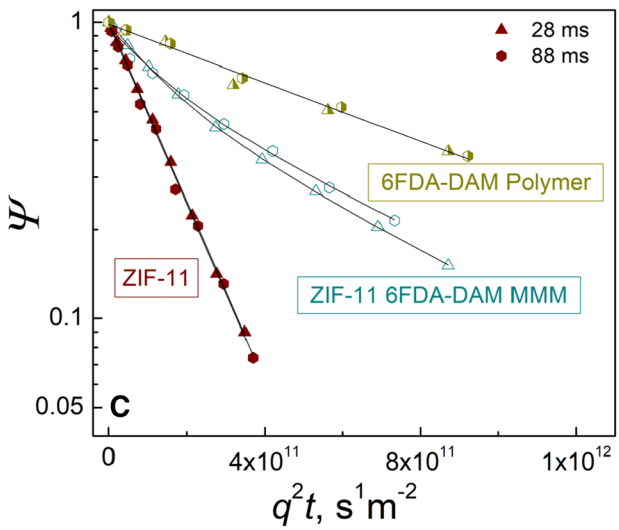

Fig. 7 Examples of a scanning electron microscopy (SEM) images of ▶ the studied MMM and of ^{13}C PFG NMR attenuation curves measured for the intra-ZIF self-diffusion of C_2H_6 at the gas loading pressure of 2.1 bar (**b**) and 0.8 (**c**) bar at 296 K. The SEM image is shown for ZIF-11/Matrimid MMM (**a**). The PFG NMR attenuation curves were measured for ZIF-11 beds (filled symbols), MMMs (hollow symbols), and the polymer film (half-filled symbols). The MMM and polymer types used in the attenuation curve measurements are indicated in the figure. The solid lines in **b** and **c** show the results of least-square fitting by using Eq. 1 for ZIF-11 crystal beds, ZIF-11/Torlon MMM, and 6FDA-DAM polymer film, and by using Eq. 3 for ZIF-11/6FDA-DAM MMM. In all cases, the small (~3–5 μm) ZIF-11 crystal batch was used

as the intra-ZIF self-diffusivity in beds of ZIF-11 crystals indicating no confinement effect for 6FDA-DAM and Matrimid polymers at all studied gas loading pressures (Fig. 8) (Forman et al. 2019, 2020). It was observed that the effect of ZIF-11 confinement in a polymer on intra-ZIF self-diffusion correlates with the polymer bulk modulus, which is larger for Torlon (4.5 GPa Basler et al. 2013; Mueller et al. 2013) than for Matrimid (3.5 GPa Kozey and Kumar 2011) and 6FDA-DAM (1.2 GPa Harding et al. 2002) polymers (Forman et al. 2019, 2020).

It is seen in Fig. 8 that the ratio of the intra-ZIF self-diffusivity in a bed of ZIF-11 crystals to that in ZIF-11/Torlon MMM approaches 1 as the gas loading pressure increases. This observation can be explained by sorbate crowding in ZIF-11 at high loading pressures resulting in a reduction in the ZIF-11 framework flexibility due to difficulties for a linker to reorient when available free volume is drastically reduced by adsorbed gas molecules. In this case, the confinement effect in Torlon does not lead to a significant reduction in the ZIF-11 framework flexibility because it is already reduced by sorbate crowding. Alternatively, the observed reduction of the confinement effect in Torlon on the gas-self-diffusivities at high gas loading pressures can also be explained by Torlon plasticization at these gas loading pressures reducing the effect of confinement exerted by the polymer on ZIF-11 crystals (Forman et al. 2019, 2020).

In order to develop a better understanding of the confinement effect in Torlon on intra-ZIF self-diffusion, temperature dependence of intra-ZIF self-diffusivity of C_2H_6 and C_2H_4 in ZIF-11/Torlon MMM was studied using ^1H and ^{13}C high field PFG NMR (Fig. 9) (Forman et al. 2020). Coincidence of the data obtained using different types of nuclei (^1H and ^{13}C) under the same conditions and for the same samples confirms absence of any measurement artifacts. To obtain diffusion data for the same or similar intra-ZIF concentrations at different temperatures, several ZIF-11/Torlon MMM samples with different sorbate loadings at ambient temperature were prepared and studied. It was observed that the temperature dependence of the self-diffusivities of C_2H_6 and C_2H_4 can be described by Arrhenius law (Fig. 9). Figure 9a shows the Arrhenius plots measured for self-diffusion of C_2H_6 in ZIF-11 crystal bed and ZIF-11/Torlon MMM. The activation energies of diffusion obtained from these plots were found to be the same for ZIF-11 bed and the MMM, within uncertainty (Baniani

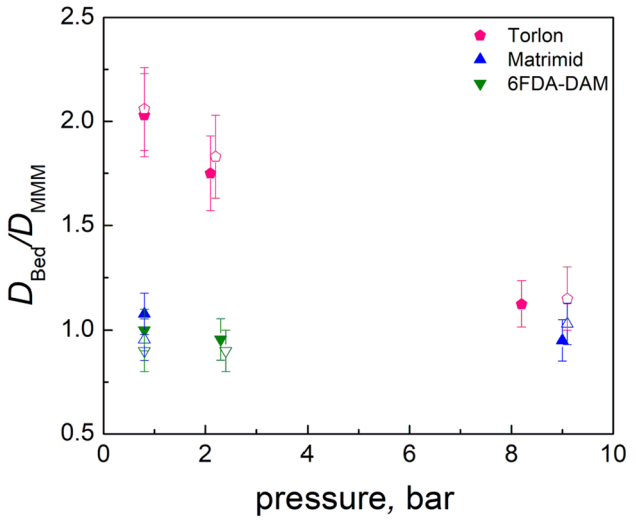

Fig. 8 Ratios of the intra-ZIF self-diffusivities of C_2H_6 (filled symbols) and C_2H_4 (hollow symbols) in ZIF-11 beds to those in ZIF-11 based MMMs measured by PFG NMR at 296 K for different sorbate loading pressures. The data were measured with the small (~3–5 μm) ZIF-11 crystal batch

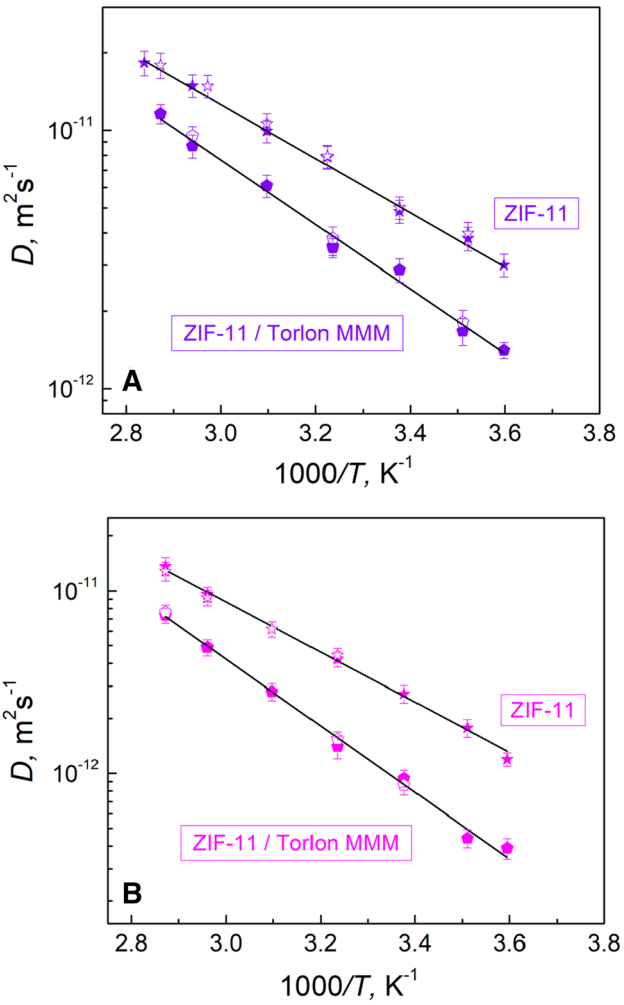

Fig. 9 Self-diffusivities of C_2H_6 (**a**) and C_2H_4 (**b**) as a function of temperature measured by PFG NMR for ZIF-11 crystal beds (star symbols) and ZIF-11/Torlon MMM (pentagon symbols). The diffusion measurements were performed using ^{1}H (filled symbols) and ^{13}C (hollow symbols) resonances under the conditions of the same or similar intra-ZIF concentrations and MSDs for each sorbate. The data were measured with the small (~3–5 μm) ZIF-11 crystal batch

et al. 2019; Forman et al. 2020). The corresponding Arrhenius plots for self-diffusion of C_2H_4 in ZIF-11 crystal bed and ZIF-11/Torlon MMM are presented in Fig. 9b. The resulting activation energy of diffusion of C_2H_4 was found to be higher for ZIF-11/Torlon MMM than that for ZIF-11 crystal bed (34.9 kJ/mol in the MMM vs. 26.3 kJ/mol in the bed) (Forman et al. 2020; Baniani et al. 2019). Such activation energy change is consistent with a reduced framework flexibility and resulting lower effective aperture size due to confinement of ZIF-11 crystals in Torlon (Forman et al. 2020). It is important to note that even without any confinement effects the presence of C_2H_4 in ZIF-11 is expected to reduce the effective or maximum aperture size in ZIF-11 (Baniani et al. 2019). At the same time, no such aperture reduction is expected due to the presence of C_2H_6 in ZIF-11. Hence, a reduction of the effective aperture size of ZIF-11 due to confinement in Torlon can have a more pronounced effect on the activation energy of diffusion for C_2H_4 than for C_2H_6, as observed experimentally, because this confinement reduces the aperture to a smaller value for the former sorbate.

Although MOF/polymer MMMs have shown promising performance in molecular separations, many limitations still exist in their applications as the selectivity, permeability and overall performance of MMMs can be strongly affected by structural defects and changes resulting from the MMM formation. In particular, pore blockage at the MOF crystal surface by polymer chains, polymer chain rigidification near the external surface of MOF crystals, and poor adhesion between the MOF crystals and polymer can affect the molecular transport in MMMs (Fang et al. 2015; Ding et al. 2018; Amooghin et al. 2019). For example, in a study of ZIF-8/PDMS MMM it is discussed that the PDMS polymer chains can get adhered to the ZIF-8 particles and cause pore blockage, which can lead to a reduction in the membrane permeability (Fang et al. 2015). Similar effect is also discussed for PEO/ZIF-8 MMM, where the partial pore blockage caused by penetration of polymer chains into the pores of ZIF-8 can decrease the overall sorbate permeability (Ding et al. 2018). Furthermore, polymer chain rigidification near the external surface of MOF crystals embedded in the polymer matrix can reduce the intra-polymer diffusivity in MMMs, as was recently demonstrated in our high field PFG NMR studies (Mueller et al. 2015, 2016; Forman et al. 2019,

2020). High field PFG NMR can also allow for direct detection of the formation of pockets of free volume due to poor adhesion between MOF crystals and a polymer in MMMs, as discussed in detail below.

Figure 10a, b shows examples of SEM images, which suggest an existence of cavities between MOF particles and the polymer phase in UiO-66–NH_2/Matrimid MMM.

It is important to note that such visible defects in the SEM images can be an artifact caused by membrane cryo-fracturing required to take a cross sectional image. Clearly, it would be advantageous to investigate the existence of such defects in membranes which are not perturbed by cryo-fracturing. To this end, we have utilized ^{1}H PFG NMR at 14 T and studied self-diffusion of *para*-xylene (*p*-xylene) and *ortho*-xylene (*o*-xylene) in the same UiO-66–NH_2/Matrimid MMM for a broad range of diffusion times. To prepare an NMR sample, a membrane film was rolled and placed into a 5 mm thin wall NMR tube to reach a height of about 30 mm. The sample was attached to a custom-made vacuum system to degas overnight at 373 K. After degassing, a sufficient amount of a sorbate was cryogenically introduced into the sample to ensure full saturation of the membrane with the liquid sorbate. Upon loading, each sample was flame sealed and removed from the vacuum system. *p*-Xylene and *o*-xylene were chosen as sorbates because proton T_2 NMR relaxation times of these molecules inside the MOF and polymer phases of the UiO-66–NH_2/Matrimid MMM were found to be prohibitively low for an observation of any PFG NMR signal in these phases under our experimental conditions. This was verified by observing no PFG NMR signal of *p*-xylene and *o*-xylene inside a bed of UiO-66–NH_2 particles and in a pure Matrimid film. Figure 10c shows examples of ^{1}H PFG NMR attenuation curves measured for the self-diffusion of the xylene isomers in UiO-66–NH_2/Matrimid MMM for a broad range of diffusion times between 29 and 299 ms at 296 K. In the presentation of this figure, coincidence of the attenuation curves measured at different diffusion times indicates independence of the root MSD of the diffusion time, thus signaling completely restricted diffusion in agreement with Eq. 4. This completely restricted diffusion was assigned to diffusion of *p*-xylene and *o*-xylene in the pockets of free volume formed around MOF particles in the MMM. Using Eq. 4, a known expression for PFG NMR attenuation in the case of a completely restricted diffusion in spherical pores of diameter d_{eff}, the value of d_{eff} was found to be equal to 0.5 ± 0.1 μm for both xylene isomers. It is seen in Fig. 10b that this value is in a reasonable agreement with the size of the cavities that can be seen in the SEM image. To our knowledge, these data represent the first direct proof of the existence of pockets of free volume in any type of MMM based on diffusion measurements.

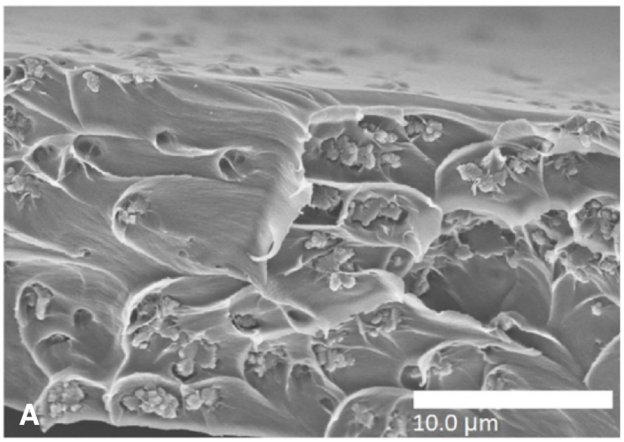

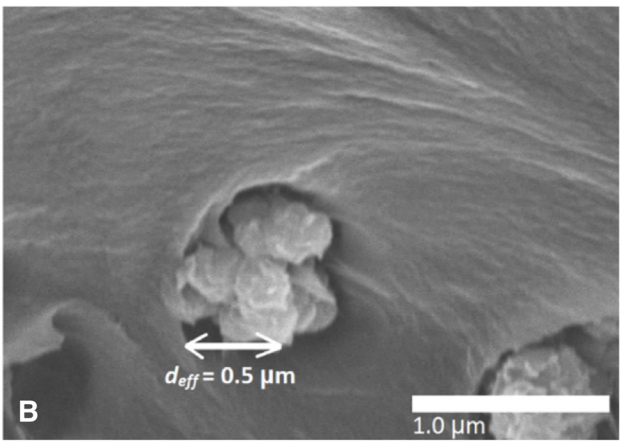

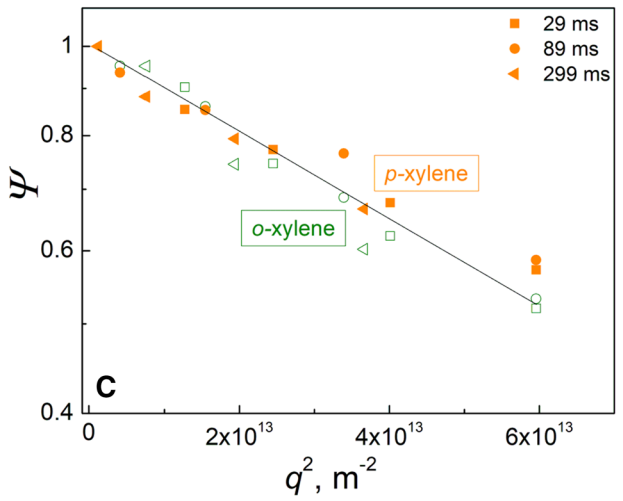

Fig. 10 Examples of the SEM images of UiO-66–NH_2/Matrimid MMM (**a**, **b**), and of ^{1}H PFG-NMR attenuation curves measured for diffusion of *p*-xylene (filled symbols) and *o*-xylene (hollow symbols) in UiO-66–NH_2/Matrimid MMM at 296 K and 14 T (**c**). The solid lines represent the results of least-square fitting using Eq. 4

5 Single-file diffusion of mixed gases

In addition to investigations of normal and restricted self-diffusion in ZIFs and mixed-matrix membranes, also studies of diffusion with anomalous diffusion mechanism in porous systems can significantly benefit from an application of high field and high gradient PFG NMR. One type of anomalous diffusion of interest is that of single-file diffusion (SFD; Kärger et al. 2012; Nelson and Auerbach 1999; Adhangale and Keffer 2003; Dutta et al. 2015). SFD occurs when nonintersecting channels are narrow enough such that they prohibit molecules from passing one another. In this mode of diffusion, molecular order within the channels is conserved. In normal diffusion, MSD depends linearly on diffusion time. In contrast, one of the hallmark features of SFD in channels sufficiently long enough to neglect any effects related to channel boundaries is that MSD increases proportionally to the square root of diffusion time (Eq. 5), where the proportionality coefficient is a single-file mobility factor (F) (Kärger et al. 2012).

The restrictive nature of this diffusion mechanism has the potential to generate highly selective separations in multi-component mixtures. Both Monte Carlo and molecular dynamics simulations have provided insights on this potential (Nelson and Auerbach 1999; Adhangale and Keffer 2003; Sholl and Fichthorn 1997b). SFD conditions can also be beneficial for heterogeneous catalysis in porous systems (Rodenbeck et al. 1995; Kärger et al. 1992; Kärger and Vasenkov 2005; Broadbelt and Snurr 2000; Neugebauer et al. 2000). One major challenge in developing such SFD-based applications is related to the difficulty of studying molecular SFD experimentally, especially when SFD needs to be observed for molecular mixtures expected under typical conditions of separations and catalysis. Although experimental investigations of SFD of single component sorbates were reported more than two decades ago (Hahn et al. 1996; Kukla et al. 1996), the corresponding studies of SFD of mixtures of different types of molecules were performed only recently owing to the availability of high field and high magnetic field gradient PFG NMR (Dutta et al. 2015, 2016). In the latter studies, the high field of 17.6 T allowed observing sufficiently large signal of diffusing molecules even when using ^{13}C PFG NMR instead of a more traditional ^{1}H PFG NMR (Dutta et al. 2015, 2016). An application of large gradients up to 23 T/m allowed obtaining diffusion data for the diffusion time range spanning around 2 orders of magnitude. More details on these SFD studies are presented below.

L-alanyl-L-valine (AV) dipeptide nanotubes with inner diameters of 0.51 nm (Soldatov et al. 2004) were chosen as a model sorbent. The channel diameter in these nanotubes is sufficiently small to expect SFD conditions for both mixed and pure CO, CO_2, and CH_4, which were selected as sorbates. Figure 11 shows examples of the ^{13}C PFG NMR attenuation curves measured for these gases in AV. In this figure, the attenuation is plotted as a function of $q^2t^{0.5}$ for both single sorbates (Fig. 11a) and mixed sorbates (Fig. 11b) to test the applicability of Eq. 6 for SFD (Dutta et al. 2015, 2016). It is seen in the figure that the attenuation curves for each sorbate type in each sorbate/AV sample overlap across a broad range of diffusion times, which is consistent with Eq. 6. When CO and CH_4 are measured as single sorbates (Fig. 11a), their attenuation curves are quite distinct from one another indicating a significantly different single-file mobility factor for each gas. However, when these gases are mixed, all attenuation curves for both sorbates overlap, thereby indicating identical self-diffusion rates for CO and CH_4 (Fig. 11b). Indeed, under the conditions of SFD,

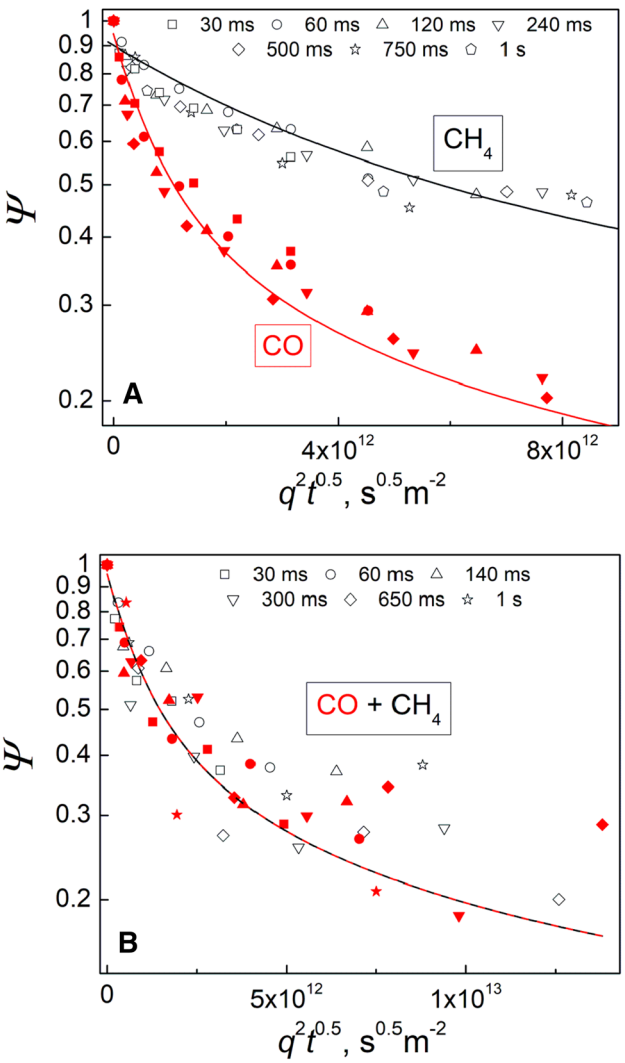

Fig. 11 Examples of ^{13}C PFG NMR attenuation curves at 298 K for CH_4 (unfilled symbols) and CO (filled symbols) in AV channels loaded with a single gas (**a**), or with an equimolar CO/CH_4 mixture (**b**). The solid lines show the best-fit lines obtained using Eq. 6

identical values of F are expected for mixtures as molecules are unable to pass one another. Qualitatively the same results were also obtained by PFG NMR for the diffusion of mixed and pure CO and CO_2 in AV (Dutta et al. 2015, 2016). Least-square fit of the combined data corresponding to all the attenuation curves measured in each sample (i.e. attenuation curves for different diffusion times and, for mixture samples, also for different gases) by Eq. 6 yielded a single value of F for each sample (Dutta et al. 2016). Solid lines in Fig. 11 show the corresponding best fit lines for the mixed and pure CO and CH_4 samples. The observation that the gas diffusion in each studied mixture sample can be characterized by a single value of F, which does not depend on the gas type, provides an additional evidence that the measured diffusion process occurs under the SFD conditions.

Further evidence of SFD in the studied AV samples is presented in Fig. 12, which shows values of MSD as a function of diffusion time for CO/CH_4 and CO/CO_2 mixtures as well as for the corresponding single sorbates. MSD values were determined from least-square fits of the PFG NMR attenuation curves at different diffusion times using Eq. 6. It is important to note that all MSD values reported in Fig. 12 correspond to displacements along the diffusion pathways in AV channels, which exhibit helical geometry (Dvoyashkin et al. 2013; Dutta et al. 2016).

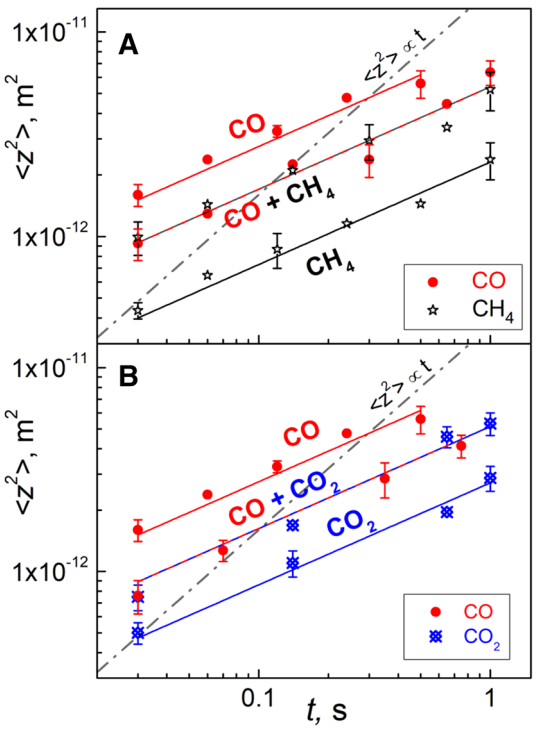

Fig. 12 Gas MSD as a function of diffusion time in AV channels at 298 K for an equimolar mixture and pure CO and CH_4 (**a**), and for an equimolar mixture and pure CO and CO_2 (**b**). Solid lines show the best-fit lines obtained using Eq. 5. Broken lines correspond to a linear dependence of MSD on time, which is expected for normal diffusion according to Eq. 2

The time dependencies of the measured MSDs in Fig. 12 were found to be in agreement with Eq. 5, thus confirming SFD. Least-square fits of the time dependencies in Fig. 12 by this equation are shown as solid lines with the slopes yielding the values of F. These values were found to be identical, within uncertainty, with the corresponding values of F obtained for each sample from fitting all the attenuation curves measured for different diffusion times and sorbate types (in the case of mixtures) together by Eq. 6, as discussed above (Dutta et al. 2016). For reference, broken lines showing linear growth of MSD with t, as expected for normal diffusion, are plotted to contrast the solid lines showing MSD that grow with $t^{0.5}$.

At sufficiently large values of MSD, computer simulations and theoretical studies of diffusion in SFD channels of finite length predict a transition from the MSD time dependence given by Eq. 5 to that of normal diffusion (Eq. 2), but with the diffusivity, which is much smaller than the corresponding diffusivity for normal diffusion where molecules can pass one another in channels (Delfau et al. 2011; Nelson and Auerbach 1999; Hahn and Kärger 1998). For such large MSDs, the time scaling of Eq. 2 becomes applicable in SFD channels because the rate of molecular transport in this case is governed by correlated movements of all molecules in each particular channel. As a result of such correlations, consecutive displacements of all molecules in each channel mimic those of one large particle made of all the molecules in a channel. As such consecutive movements are expected to be independent of one another, the MSD grows linearly with t (Delfau et al. 2011; Nelson and Auerbach 1999; Hahn and Kärger 1998). Such diffusion regime in SFD channels is often referred to as a center-of-mass (COM) diffusion regime. If SFD is modelled as a random walk with particles behaving as hard spheres, the transition from SFD to COM is expected to happen for the crossover MSD value equal to $\left(\frac{1-\theta}{\theta}\right)\left(\frac{2l\lambda}{\pi}\right)$, where θ is the fractional loading in channels, l is the channel length, and λ is the particle elementary displacement, which is also equal to the particle size (Hahn and Kärger 1998; Nelson and Auerbach 1999). This relation predicts a crossover MSD, which is in all cases smaller than the smallest MSD values measured in the discussed above PFG NMR studies of gas diffusion in AV channels. However, the PFG NMR data for these channels showed the MSD time scaling of SFD in agreement with Eq. 5. This apparent conflict between the theoretical prediction and experimental results can be reconciled if one accounts for interactions between molecules, wherein they form molecular clusters. In fact, molecular-level simulations indicate that self-diffusion in one-dimensional channels can occur via movements of molecular clusters, which form due to intermolecular

interactions (Sholl 1999; Sholl and Fichthorn 1997a; Sholl and Lee 2000). This implies that the originally assumed λ values equal to the size of individual gas molecules in AV channels are actually much larger. Obtaining the crossover MSD larger than the largest measured MSD in AV channels requires the values of λ corresponding to the size of clusters between 30 and 140 gas molecules of the types used in the PFG NMR measurements (Dutta et al. 2016, 2018b). Hence, the assumption about the existence of such molecular clusters allows reconciling the experimental data discussed above for the SFD of mixed and pure gases in AV channels with the expectation of the crossover to the COM regime at sufficiently large MSD values. This assumption was also found to be in agreement with the observation of larger values of F for pure CO than those for pure CO_2 and CH_4 in AV for the same or similar loadings and temperature (Dutta et al. 2016, 2018b). Indeed, as discussed in Dutta et al. (2016, 2018b) formation of larger clusters should lead to larger values of F for the same loading and temperature. Owing to dipole–dipole interactions between CO molecules and the absence of such or similarly strong interactions for the other two studied gases, larger clusters are expected for CO. This should result in larger F for CO, as observed experimentally (Dutta et al. 2015, 2016). In summary, high field NMR with large magnetic field gradients offered a unique ability to observe mixed-gases in the SFD regime. This allowed bringing multicomponent SFD from theoretical predictions into the world of experimentally observed phenomena.

6 Conclusion

The PFG NMR studies reviewed in this paper benefited from enhanced signal-to-noise ratios resulting from large (up to 17.6 T) applied magnetic fields in combination with shortened time windows in PFG NMR pulse sequences during which the signal was reduced by the T_2 NMR relaxation process. Such time window decrease was possible due to the use of large (up to 25 T/m) magnetic field gradients. Large gradients also allowed pushing the limits of the smallest diffusion length scale for which diffusion data can still be reliably measured. The highly restrictive nature of nanopore environments can often cause sorbates to have prohibitively short proton T_2 NMR relaxation times, which can preclude measurement by ^{1}H PFG NMR. However, high field NMR allows using nuclei types with an intrinsically low sensitivity (^{13}C and ^{129}Xe), which have a benefit of typically larger T_2 NMR relaxation times even under the conditions of extreme confinement. ^{13}C and ^{129}Xe also exhibit large T_1 NMR relaxation times, which allow expanding the range of diffusion times used in PFG NMR measurements. As a result, utilizing these nuclei types allowed overcoming the signal-to-noise and diffusion time range limitations, which are often observed in ^{1}H PFG NMR measurements.

The high field PFG NMR technique provided insights on a variety of self-diffusion processes; it was used to study and differentiate between normal, anomalous, and restricted types of diffusion in porous solids. For example, the observation of normal diffusion of C_2H_6 and C_2H_4 revealed an atypical relationship between these sorbates' self-diffusivities in which intra-ZIF self-diffusivity of larger C_2H_6 was higher than that of smaller C_2H_4. This anomalous relationship between the self-diffusivity and molecular size is explained by the reduction in ZIF framework flexibility caused by C_2H_4 interaction with the ZIF-11 framework. Separately, high field diffusion NMR illuminated a different effect of framework flexibility on diffusion in mixed-linker ZIF-7–8, wherein increasing size of gas molecules larger than CO_2 appear to induce larger framework distortions facilitating the self-diffusion process. Furthermore, analysis of the PFG NMR data for ZIF-7–8 led to the conclusion about a distribution of self-diffusivities within the crystal bed consistent with uniform transport properties in any particular ZIF-7–8 crystal, but different self-diffusivities in different crystals. This conclusion was confirmed by single crystal IRM diffusion measurements.

Further observation of diffusion effects linked to ZIF framework flexibility were made by high field PFG NMR for ZIF-11 crystals confined in Torlon polymer. The crystal confinement in the polymer was found to be capable of reducing sorbates' intra-ZIF self-diffusivities and increasing the activation energy of diffusion. These changes in the self-diffusion properties were explained by a reduction in ZIF-11 framework flexibility under the conditions of crystal confinement in the polymer.

Moreover, it was demonstrated that high field PFG NMR can be used successfully to study both restricted and anomalous diffusion. In particular, PFG NMR allowed measuring the *o*- and *p*-xylene self-diffusion, which was observed to be completely restricted inside interfacial voids formed in UiO-66–NH_2/Matrimid mixed-matrix membrane. Additionally, multi-sorbate single-file diffusion—a well-known type of anomalous diffusion—was experimentally observed and investigated for the first time for molecular mixtures.

Acknowledgements We are grateful for the financial support of this work by NSF (Award Nos. 1836735, 1836738, and 1561347). A portion of this work was performed in the McKnight Brain Institute at the National High Magnetic Field Laboratory's AMRIS Facility, which is supported by National Science Foundation Cooperative Agreement No. DMR-1157490 and the State of Florida. This work was supported in part by an NIH Award, S10RR031637, for magnetic resonance instrumentation. The IRM measurements were performed at Leipzig University.

Author contributions AB and SJB have contributed equally to this work.

Funding Financial support received from the National Science Foundation and National Institutes of Health.

Data availability Not applicable.

Code availability Not applicable.

Compliance with ethical standards

Conflicts of interest The authors declare no conflict of interest.

References

Adhangale, P., Keffer, D.: Exploiting single-file motion in one-dimensional nanoporous materials for hydrocarbon separation. Sep. Sci. Technol. **38**(5), 977–998 (2003). https://doi.org/10.1081/ss-120018119

Amooghin, A.E., Mashhadikhan, S., Sanaeepur, H., Moghadassi, A., Matsuura, T., Ramakrishna, S.: Substantial breakthroughs on function-led design of advanced materials used in mixed matrix membranes (MMMs): a new horizon for efficient CO_2 separation. Prog. Mater. Sci. **102**, 222–295 (2019)

Bae, T.-H., Lee, J.S., Qiu, W., Koros, W.J., Jones, C.W., Nair, S.: A high-performance gas-separation membrane containing submicrometer-sized metal–organic framework crystals. Angew. Chem. Int. Ed. **49**(51), 9863–9866 (2010)

Baker, R.W.: Future directions of membrane gas separation technology. Ind. Eng. Chem. Res. **41**(6), 1393–1411 (2002)

Banerjee, D., Elsaidi, S.K., Thallapally, P.K.: Xe adsorption and separation properties of a series of microporous metal–organic frameworks (MOFs) with V-shaped linkers. J. Mater. Chem. A **5**(32), 16611–16615 (2017). https://doi.org/10.1039/c7ta02746j

Banerjee, R., Phan, A., Wang, B., Knobler, C., Furukawa, H., O'Keeffe, M., Yaghi, O.M.: High-throughput synthesis of zeolitic imidazolate frameworks and application to CO_2 capture. Science **319**, 939–943 (2008). https://doi.org/10.1126/science.1152516

Baniani, A., Chmelik, C., Forman, E.M., Fan, L., Ziegler, K.J., Zhou, E., Zhang, F., Lyndon, R., Lively, R.P., Vasenkov, S.: Anomalous relationship between molecular size and diffusivity of ethane and ethylene inside crystals of zeolitic imidazolate framework-11. J. Phys. Chem. C **123**(27), 16813–16822 (2019)

Basler, S.E., Traxler, J., Müller, R., Lenthe, G.H.V.: Peri-implant bone microstructure determines dynamic implant cut-out. Med. Eng. Phys. **35**(10), 1442–1449 (2013)

Berens, S., Chmelik, C., Hillman, F., Kärger, J., Jeong, H.-K., Vasenkov, S.: Ethane diffusion in mixed linker zeolitic imidazolate framework-7–8 by pulsed field gradient NMR in combination with single crystal IR microscopy. Phys. Chem. Chem. Phys. **20**, 23967–23975 (2018)

Berens, S., Hillman, F., Jeong, H.-K., Vasenkov, S.: Self-diffusion of pure and mixed gases in mixed-linker zeolitic imidazolate framework-7–8 by high field diffusion NMR. Microporous Mesoporous Mater. **288**, 109603 (2019)

Bernardo, P., Drioli, E., Golemme, G.: Membrane gas separation: a review/state of the art. Ind. Eng. Chem. Res. **48**, 4638–4663 (2009)

Broadbelt, L.J., Snurr, R.Q.: Applications of molecular modeling in heterogeneous catalysis research. Appl. Catal. A **200**(1–2), 23–46 (2000)

Callaghan, P.T.: Translational Dynamics and Magnetic Resonance, 1st edn. Oxford University Press, Oxford (2011)

Callaghan, P.T., MacGowan, D., Packer, K.J., Zelaya, F.O.: Influence of field gradient strength in NMR studies of diffusion in porous media. Magn. Reson. Imaging **9**, 663–671 (1991)

Delfau, J.B., Coste, C., Saint Jean, M.: Single-file diffusion of particles with long-range interactions: damping and finite-size effects. Phys. Rev. E **84**(1 Pt 1), 011101 (2011). https://doi.org/10.1103/PhysRevE.84.011101

Díaz, K., López-González, M., del Castillo, L.F., Riande, E.: Effect of zeolitic imidazolate frameworks on the gas transport performance of ZIF8-poly (1,4-phenylene ether-ether-sulfone) hybrid membranes. J. Membr. Sci. **383**, 206–213 (2011)

Diestel, L., Wang, N., Schwiedland, B., Steinbach, F., Giese, U., Caro, J.: MOF based MMMs with enhanced selectivity due to hindered linker distortion. J. Membr. Sci. **492**, 181–186 (2015)

Ding, X., Li, X., Zhao, H., Wang, R., Zhao, R., Li, H., Zhang, Y.: Partial pore blockage and polymer chain rigidification phenomena in PEO/ZIF-8 mixed matrix membranes synthesized by in situ polymerization. Chin. J. Chem. Eng. **26**(3), 501–508 (2018)

Dutta, A., Tymińska, N., Zhu, G., Collins, J., Lively, R.P., Schmidt, J.R., Vasenkov, S.: Influence of hydrogen sulfide exposure on the transport and structural properties of the metal–organic framework ZIF-8. J. Phys. Chem. C **122**(13), 7278–7287 (2018a)

Dutta, A.R., Sekar, P., Dvoyashkin, M., Bowers, C., Ziegler, K.J., Vasenkov, S.: Possible role of molecular clustering in single-file diffusion of mixed and pure gases in dipeptide nanochannels. Microporous Mesoporous Mater. **269**, 83–87 (2018b)

Dutta, A.R., Sekar, P., Dvoyashkin, M., Bowers, C.R., Ziegler, K.J., Vasenkov, S.: Relationship between single-file diffusion of mixed and pure gases in dipeptide nanochannels by high field diffusion NMR. Chem. Commun. **51**, 13346–13349 (2015)

Dutta, A.R., Sekar, P., Dvoyashkin, M., Bowers, C.R., Ziegler, K.J., Vasenkov, S.: Single-file diffusion of gas mixtures in nanochannels of the dipeptide l-Ala-l-Val: high-field diffusion NMR study. J. Phys. Chem. C **120**(18), 9914–9919 (2016)

Dvoyashkin, M., Wang, A., Vasenkov, S., Bowers, C.R.: Xenon in l-alanyl-l-valine nanochannels: a highly ideal molecular single-file system. J. Phys. Chem. Lett. **4**(19), 3263–3267 (2013). https://doi.org/10.1021/jz4016712

Eum, K., Jayachandrababu, K.C., Rashidi, F., Zhang, K., Leisen, J., Graham, S., Lively, R.P., Chance, R.R., Sholl, D.S., Jones, C.W., Nair, S.: Highly tunable molecular sieving and adsorption properties of mixed-linker zeolitic imidazolate frameworks. J. Am. Chem. Soc. **137**(12), 4191–4197 (2015). https://doi.org/10.1021/jacs.5b00803

Fang, M., Wu, C., Yang, Z., Wang, T., Xia, Y., Li, J.: ZIF-8/PDMS mixed matrix membranes for propane/nitrogen mixture separation: experimental result and permeation model validation. J. Membr. Sci. **474**, 103–113 (2015)

Forman, E.M., Baniani, A., Fan, L., Ziegler, K.J., Zhou, E., Zhang, F., Lively, R.P., Vasenkov, S.: Ethylene diffusion in crystals of zeolitic imidazole framework-11 embedded in polymers to form mixed-matrix membranes. Microporous Mesoporous Mater. **274**, 163–170 (2019)

Forman, E.M., Baniani, A., Fan, L., Ziegler, K.J., Zhou, E., Zhang, F., Lively, R.P., Vasenkov, S.: Relationship between ethane and ethylene diffusion inside ZIF-11 crystals confined in polymers to form mixed-matrix membranes. J. Membr. Sci. **593**, 117440 (2020)

Forman, E.M., Pimentel, B.R., Ziegler, K.J., Lively, R.P., Vasenkov, S.: Microscopic diffusion of pure and mixed methane and carbon dioxide in ZIF-11 by high field diffusion NMR. Microporous Mesoporous Mater. **248**, 158–163 (2017)

Freude, D., Dvoyashkina, N., Arzumanov, S.S., Kolokolov, D.I., Stepanov, A.G., Chmelik, C., Jin, H., Li, Y., Kärger, J., Haase, J.: NMR study of the host structure and guest dynamics investigated

with alkane/alkene mixtures in metal organic frameworks ZIF-8. J. Phys. Chem. C **123**(3), 1904–1912 (2019)
Hahn, K., Kärger, J.: Deviations from the normal time regime of single-file diffusion. J. Phys. Chem. B **102**, 5766–5771 (1998)
Hahn, K., Kärger, J., Kukla, V.: Single-file diffusion observation. Phys. Rev. Lett. **76**(15), 2762–2765 (1996)
Haldoupis, E., Watanabe, T., Nair, S., Sholl, D.S.: Quantifying large effects of framework flexibility on diffusion in MOFs: CH_4 and CO_2 in ZIF-8. ChemPhysChem Eur. J. Chem. Phys. Phys. Chem. **13**(15), 3449–3452 (2012). https://doi.org/10.1002/cphc.201200529
Harding, D., Tsai, F.Y., Gram, R.Q.: The properties of polyimide targets. LLE Rev. **92**, 167–180 (2002)
Hillman, F., Brito, J., Jeong, H.K.: Rapid one-pot microwave synthesis of mixed-linker hybrid zeolitic-imidazolate framework membranes for tunable gas separations. ACS Appl. Mater. Interfaces **10**(6), 5586–5593 (2018). https://doi.org/10.1021/acsami.7b18506
Hillman, F., Zimmerman, J.M., Paek, S.-M., Hamid, M.R.A., Lim, W.T., Jeong, H.-K.: Rapid microwave-assisted synthesis of hybrid zeolitic–imidazolate frameworks with mixed metals and mixed linkers. J. Phys. Chem. A **5**(13), 6090–6099 (2017). https://doi.org/10.1039/c6ta11170j
Kärger, J., Avramovska, M., Freude, D., Haase, J., Hwang, S., Valiullin, R.: Pulsed field gradient NMR diffusion measurement in nanoporous materials. In: Adsorption. Springer (2020)
Kärger, J., Petzold, M., Pfeifer, H., Ernst, S., Weitkamp, J.: Single-file diffusion and reaction in zeolites. J. Catal. **136**(2), 283–299 (1992). https://doi.org/10.1016/0021-9517(92)90062-m
Kärger, J., Pfeifer, H., Heink, W.: Principles and application of self-diffusion measurements by NMR. Adv. Magn. Reson. **12**, 1–89 (1988)
Kärger, J., Ruthven, D.M., Theodorou, D.N.: Diffusion in Nanoporous Materials. Wiley-VCH Verlag GmbH and Co. KGaA, Weinheim (2012)
Kärger, J., Vasenkov, S.: Quantitation of diffusion in zeolite catalysts. Microporous Mesoporous Mater. **85**(3), 195–206 (2005)
Kärger, J., Vasenkov, S., Auerbach, S.M.: Diffusion in zeolites. In: Auerbach, S.M. (ed.) Handbook of Zeolite Science and Technology, pp. 341–422, Marcel Dekker, Inc., New York (2003)
Kortunov, P., Ni, Z., Paur, C., Reyes, S., Zengel, J.: Loading-dependent transport properties of zeolitic imidazolate frameworks probed by in-situ PFG NMR. AIP Conf. Proc. **1330**, 57–60 (2011)
Kozey, V.V., Kumar, S.: Compression behavior of materials: Part I. Glassy polymers. J. Mater. Res. **9**(10), 2717–2726 (2011)
Kukla, V., Kornatowski, J., Demuth, D., Girnus, I., Pfeifer, H., Rees, L.V.C., Schunk, S., Unger, K.K., Kärger, J.: NMR studies of single-file diffusion in unidimensional channel zeolites. Science **272**(5262), 702–704 (1996)
Li, J.-R., Kuppler, R.J., Zhou, H.-C.: Selective Gas Adsorption and separation in metal–organic frameworks. Chem. Soc. Rev. **38**, 1477–1504 (2009). https://doi.org/10.1039/b802426j
Li, T., Pan, Y., Peinemann, K.-V., Lai, Z.: Carbon dioxide selective mixed matrix composite membrane containing ZIF-7 nano-fillers. J. Membr. Sci. **425–426**, 235–242 (2013)
Mueller, R., Hariharan, V., Zhang, C., Lively, R., Vasenkov, S.: Relationship between mixed and pure gas self-diffusion for ethane and ethene in ZIF-8/6FDA-DAM mixed-matrix membrane by pulsed field gradient NMR. J. Membr. Sci. **499**, 12–19 (2016)
Mueller, R., Zhang, S., Zhang, C., Lively, R.P., Vasenkov, S.: Relationship between long-range diffusion and diffusion in the ZIF-8 and polymer phases of mixed-matrix membrane by high field NMR diffusometry. J. Membr. Sci. **477**, 123–130 (2015)
Mueller, T.L., Basler, S.E., Müller, R., van Lenthe, G.H.: Time-lapsed imaging of implant fixation failure in human femoral heads. Med. Eng. Phys. **35**(5), 636–643 (2013)
Nelson, P.H., Auerbach, S.M.: Modeling tracer counter-permeation through anisotropic zeolite membranes: from mean field theory to single-file diffusion. Chem. Eng. J. **74**(1–2), 43–56 (1999). https://doi.org/10.1016/s1385-8947(99)00052-2
Neugebauer, N., Bräuer, P., Kärger, J.: Reactivity enhancement by molecular traffic control. J. Catal. **194**(1), 1–3 (2000)
Ordoñez, M.J.C., Balkus Jr., K.J., Ferraris, J.P., Musselman, I.H.: Molecular sieving realized with ZIF-8/Matrimid® mixed-matrix membranes. J. Membr. Sci. **361**, 28–37 (2010)
Pandey, P., Chauhan, R.S.: Membranes for gas separation. Prog. Polym. Sci. **26**, 853–393 (2001)
Pantatosaki, E., Megariotis, G., Pusch, A.-K., Chmelik, C., Stallmach, F., Papadopoulos, G.K.: On the impact of sorbent mobility on the sorbed phase equilibria and dynamics: a study of methane and carbon dioxide within the zeolite imidazolate framework-8. J. Phys. Chem. A **116**(1), 201–207 (2011). https://doi.org/10.1021/jp207771s
Park, K.S., Ni, Z., Côté, A.P., Choi, J.Y., Huang, R., Uribe-Romo, F.J., Chae, H.K., O'Keeffe, M., Yaghi, O.M.: Exceptional chemical and thermal stability of zeolitic imidazolate frameworks. Proc. Natl Acad. Sci. USA **103**(27), 10186–10191 (2006)
Parkes, M.V., Demir, H., Teich-McGoldrick, S.L., Sholl, D.S., Greathouse, J.A., Allendorf, M.D.: Molecular dynamics simulation of framework flexibility effects on noble gas diffusion in HKUST-1 and ZIF-8. Microporous Mesoporous Mater. **194**, 190–199 (2014). https://doi.org/10.1016/j.micromeso.2014.03.027
Phan, A., Doonan, C.J., Uribe-Romo, F.J., Knobler, C.B., O'Keeffe, M., Yaghi, O.M.: Synthesis, structure, and carbon dioxide capture properties of zeolitic imidazolate frameworks. Acc. Chem. Res. **43**(1), 58–67 (2010). https://doi.org/10.1021/ar900116g
Pimentel, B.R., Jue, M.L., Zhou, E.-K., Verploegh, R.J., Leisen, J., Sholl, D.S., Lively, R.P.: Sorption and transport of vapors in ZIF-11: adsorption, diffusion, and linker flexibility. J. Phys. Chem. C **123**(20), 12862–12870 (2019)
Price, W.S.: NMR Studies of Translational Motion: Principles and Applications, 1st edn. Cambridge University Press, Cambridge (2009)
Rodenbeck, C., Kärger, J., Hahn, K.: Tracer exchange and catalytic reaction in single-file systems. J. Catal. **157**(2), 656–664 (1995). https://doi.org/10.1006/jcat.1995.1331
Sánchez-Laínez, J., Zornoza, B., Mayoral, Á., Berenguer-Murcia, Á., Cazorla-Amorós, D., Téllez, C., Coronas, J.: Beyond the H_2/CO_2 upper bound: one-step crystallization and separation of nano-sized ZIF-11 by centrifugation and its application in mixed matrix membranes. J. Mater. Chem. A **3**(12), 6549–6556 (2015)
Sholl, D.S.: Characterization of molecular cluster diffusion in $AlPO_4$-5 using molecular dynamics. Chem. Phys. Lett. **305**(3–4), 269–275 (1999). https://doi.org/10.1016/s0009-2614(99)00370-x
Sholl, D.S., Fichthorn, K.A.: Concerted diffusion of molecular clusters in a molecular sieve. Phys. Rev. Lett. **79**(19), 3569–3572 (1997a). https://doi.org/10.1103/PhysRevLett.79.3569
Sholl, D.S., Fichthorn, K.A.: Normal, single-file, and dual-mode diffusion of binary adsorbate mixtures in $AlPO_4$-5. J. Chem. Phys. **107**(11), 4384–4389 (1997b). https://doi.org/10.1063/1.474779
Sholl, D.S., Lee, C.K.: Influences of concerted cluster diffusion on single-file diffusion of CF_4 in $AlPO_4$-5 and Xe in $AlPO_4$-31. J. Chem. Phys. **112**(2), 817–824 (2000). https://doi.org/10.1063/1.480610
Soldatov, D.V., Moudrakovski, I.L., Ripmeester, J.A.: Dipeptides as microporous materials. Angew. Chem. Int. Ed. **43**(46), 6308–6311 (2004). https://doi.org/10.1002/anie.200460952
Stallmach, F., Kärger, J.: The potentials of pulsed field gradient NMR for investigation of porous media. Adsorption **5**, 117–133 (1999)
Stilbs, P.: Diffusion and Electrophoretic NMR. De Gruyter, Berlin (2019)

Thompson, J.A., Blad, C.R., Brunelli, N.A., Lydon, M.E., Lively, R.P., Jones, C.W., Nair, S.: Hybrid zeolitic imidazolate frameworks: controlling framework porosity and functionality by mixed-linker synthesis. Chem. Mater. **24**, 1930–1936 (2012). https://doi.org/10.1021/cm3006953

Torres, A.M., Pileio, G., Price, W.S.: Chapter 16: Q-space Singlet NMR. In: Long-Lived Nuclear Spin Order: Theory and Applications, pp. 302–319. The Royal Society of Chemistry (2020)

Yilmaz, G., Keskin, S.: Predicting the performance of zeolite imidazolate framework/polymer mixed matrix membranes for CO_2, CH_4, and H_2 separations using molecular simulations. Ind. Eng. Chem. Res. **51**, 14218–14228 (2012)

Zhang, C., Dai, Y., Johnson, J.R., Karvan, O., Koros, W.J.: High performance ZIF-8/6FDA-DAM mixed matrix membrane for propylene/propane separations. J. Membr. Sci. **389**, 34–42 (2012a)

Zhang, C., Lively, R.P., Zhang, K., Johnson, J.R., Karvan, O., Koros, W.J.: Unexpected molecular sieving properties of zeolitic imidazolate framework-8. J. Phys. Chem. Lett. **3**, 2130–2134 (2012b). https://doi.org/10.1021/jz300855a

Zhang, Y., Musselman, I.H., Ferraris, J.P., Balkus Jr., K.J.: Gas permeability properties of Matrimid® membranes containing the metal–organic framework Cu-BPY-HFS. J. Membr. Sci. **313**(1–2), 170–181 (2008)

Zornoza, B., Seoane, B., Zamaro, J.M., Téllez, C., Coronas, J.: Combination of MOFs and zeolites for mixed-matrix membranes. ChemPhysChem Eur. J. Chem. Phys. Phys. Chem. **12**(15), 2781–2785 (2011)

Publisher's Note Springer Nature remains neutral with regard to jurisdictional claims in published maps and institutional affiliations.